LBNL-40774
UC-419

ERNEST ORLANDO LAWRENCE
BERKELEY NATIONAL LABORATORY

The Solenoidal Transport Option: IFE Drivers, Near Term Research Facilities, and Beam Dynamics

E.P. Lee and R.J. Briggs

Accelerator and Fusion Research Division

September 1997

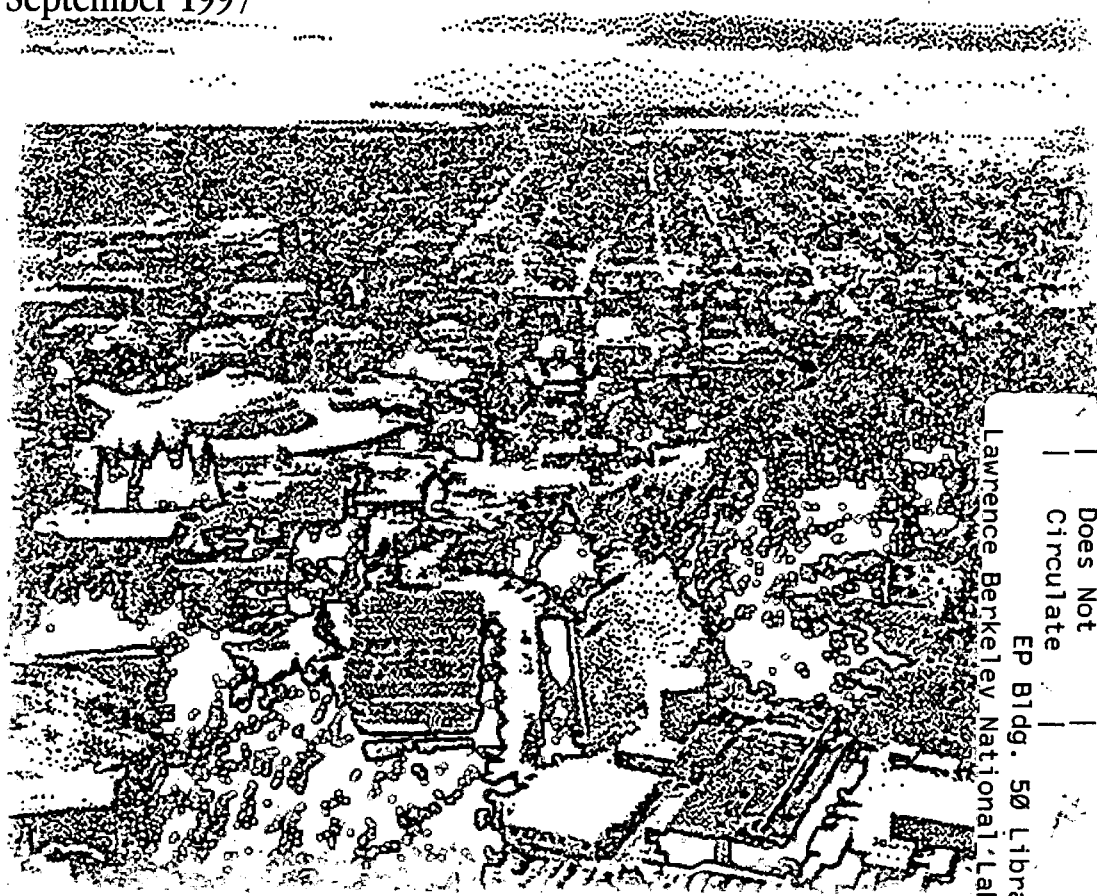

DISCLAIMER

LBNL-40774
UC-419
HIFAN 914

THE SOLENOIDAL TRANSPORT OPTION: IFE DRIVERS, NEAR TERM RESEARCH FACILITIES, AND BEAM DYNAMICS

E. P. Lee
Accelerator & Fusion Research Division
Ernest Orlando Lawrence Berkeley National Laboratory
University of California
1 Cyclotron Road, MS 47-112
Berkeley, California 94720

R. J. Briggs
Science Applications International Corporation
5000 Hopyard Road, Suite 350
Pleasanton, California 94588

September 1997

This work was supported by the Director, Office of Energy Research, Office of Fusion Energy, of the U.S. Department of Energy under Contract No. DE–AC03–76SF00098.

THE SOLENOIDAL TRANSPORT OPTION: IFE DRIVERS, NEAR TERM RESEARCH FACILITIES, AND BEAM DYNAMICS

E. P. Lee and R. J. Briggs

September 1997

Contents

1. Introduction

Solenoidal magnets have been used as the beam transport system in all the high current electron induction accelerators that have been built in the past several decades. They have also been considered for the front end transport system for heavy ion accelerators for Inertial Fusion Energy (IFE) drivers, but this option has received very little attention in recent years. The analysis reported here was stimulated mainly by the recent effort to define an affordable "Integrated Research Experiment" (IRE) that can meet the near term needs of the IFE program. The 1996 FESAC IFE review panel agreed that an integrated experiment is needed to fully resolve IFE heavy ion driver science and technology issues; specifically, "the basic beam dynamics issues in the accelerator, the final focusing and transport issues in a reactor-relevant beam parameter regime, and the target heating phenomenology". The development of concepts that can meet these technical objectives and still stay within the severe cost constraints all new fusion proposals will encounter is a formidable challenge.

Solenoidal transport has a very favorable scaling as the particle mass is decreased (the main reason why it is preferred for electrons in the region below 50 MeV). This was recognized in a recent conceptual study of high intensity induction linac-based proton accelerators for Accelerator Driven Transmutation Technologies, where solenoidal transport was chosen for the front end [1]. Reducing the ion mass is an obvious scaling to exploit in an IRE design, since the output beam voltage will necessarily be much lower than that of a full scale driver, so solenoids should certainly be considered as one option for this experiment as well. A testbed using solenoidal transport could in principle provide a high degree of flexibility, enabling experimental studies with a range of ion masses, since it has no required periodicity tied to the ion mass. This flexibility could be exploited to study a broad parameter range in the physics of target chamber transport and target heating, for example. It is also worth noting that a significant industrial capability in superconducting solenoidal magnets exists because of applications like Magnetic Resonance Imaging (MRI); this capability could be a significant advantage in the effort to find a cost-effective approach to an IRE.

The use of solenoids for an IRE would have limited appeal if the physics and technology were unrelated to a full scale driver. There is no question that the major fraction of a full scale heavy ion driver's transport system (the high energy section) would consist of superconducting magnetic quadrupoles. In the past it has often been argued that since the low energy front end would have little influence on the overall cost of a driver, optimization of this section was lower priority. A central contention of this paper is that a "front end" design based on solenoidal transport can form the basis of a significantly different overall driver architecture. With a solenoidal front end, we can consider drivers with a much smaller number of beam channels (even one!), and eliminate beam combining. The "standard architecture" based on accelerating large numbers of beams in parallel that are combined in groups at one or more locations as they pass through the accelerator is contrasted with a "few beam, no combining" architecture in Section 3.

Historically, it was felt in the early years of the IFE program that a division of the driver output into multiple beams, on the order of 32, and particle energies of 10 GeV or more were needed for "vacuum" transport and focusing of the heavy ion beam energy onto the pellet in the reactor chamber. An implicit assumption in our thinking about alternate accelerator architectures is that one of the "novel" focusing and transport schemes compatible with liquid-wall reactor concepts will be proven viable. Within this framework, which could lead to a much more attractive overall fusion reactor concept, reduction of the number of beamlines, final focusing elements, and reactor port access holes (to 2-4) are all highly desirable features. On the other hand, if it does turn out that vacuum final focusing is required, acceleration of a small number of beams could still be used if beam splitting prior to final focus proves feasible.

A single solenoidal channel transporting a high line charge density does have a (relatively) higher risk of emittance dilution from space charge effects. The main goal of this technical note is to develop the concept of this alternate approach to a driver and to the IRE. More work is needed before it is clear that this is the best path to take, and what the baseline parameter set should be for IRE (or a driver). On the other hand, the near term R&D program to support construction of a solenoid-based IRE design would differ significantly from an electrostatic quad-based multiple beam IRE, so the time scale for decisions is not that far in the future.

In Section 2, we summarize the beam transport scaling relations in the various focusing channels, and in Section 3 we show how the transport and beam combining limitations lead to major differentiations between multiple beam driver architectures with electrostatic quadrupole focused front ends, and solenoidal front ends. In Section 4, a "strawman" IRE parameter set is presented, with rough indications on the costs of the accelerator for such a facility. Detailed presentation of the transport physics in solenoidal magnetic fields is covered in Section 5.

2. Beam Transport Scaling Laws

From Section 5, the line charge density of a space charge dominated nonrelativistic beam of radius "a" transported in a continuous solenoidal is given by (MKSA units)

$$\lambda = \frac{\pi\varepsilon_0 qe B^2 a^2}{2M} \quad , \tag{1}$$

where B is the magnetic field, M is the ion mass, and qe is the ion charge. The model is that of a uniform density beam injected into the solenoidal field from a field-free ion source, the well known Brillouin flow condition that corresponds to the maximum line charge density that can be transported for that magnetic field strength. A similar relation holds for a series of solenoidal lenses that have a periodic axial variation in B on a scale length small compared to the cyclotron wavelength, if we replace B^2 by its average value. This situation applies, for example, to interruptions in the solenoids from the accelerating gaps.

Numerically,

$$\lambda = 10\left(\frac{133q}{A}\right)B^2a^2 \quad \mu C/m \quad , \tag{2}$$

where A is the ion mass in amu, B is in Tesla, and a is in meters. From this formula, it appears that heavy ion beams with $\lambda \approx 10\ \mu C/m$ are transportable using high fields and large beam radii.

The radial potential drop across the beam is $\delta\phi \equiv \lambda/4\pi\varepsilon_0$, and the ratio of $\delta\phi$ to the beam edge voltage V is equal to the dimensionless perveance, Q. In Brillouin flow, the axial velocity is a constant across the beam, equal to

$$v_z^2 = v_0^2 - qe\lambda/2\pi\varepsilon_0 M \quad , \tag{3}$$

for a beam filling the tube, where $Mv_0^2/2 = qeV$. Since the beam current is given by $I = \lambda v_z$, it is easy to show that there is a maximum value of the current that can be transported, corresponding to a maximum perveance of $Q = 2/3$. This limiting current can be a significant factor in determining

the minimum gun voltage for injection into a solenoidal channel designed to carry very high line charge densities.

In an electrostatic quadrupole channel, the maximum line charge that can be transported is independent of the ion mass and the beam voltage. For an optimized design, it depends only on the voltage between adjacent electrodes φ_{es} and the longitudinal occupancy fraction of the quadrupole field η ;

$$\lambda \approx 0.5\,\eta\left(\frac{\varphi_{es}}{140\times10^{3}}\right)\quad \mu C/m \quad , \tag{4}$$

Typically, the limitations of voltage holding between the electrodes limit the transportable line charge density in each electrostatic quadrupole to less than 0.25 microcolombs per meter.

In an optimized magnetic quadrupole channel,

$$\lambda \approx 10\eta Ba\sqrt{\frac{V}{1.0\times10^{6}}}\sqrt{\frac{133q}{A}}\quad \mu C/m \quad , \tag{5}$$

where "a" is the maximum beam edge radius, and $B = B'a$ is the quadrupole field strength at the beam edge. This rather large transportable line charge density is constrained somewhat at low energy by the difficulty in packaging the quadrupoles into the available longitudinal space; for example, $\eta \le 0.25$ is typical at 2MV. In addition, the aspect ratio L_{field}/a should be kept larger than 3 or so to control fringe field aberrations and degradation of the effective quadrupole gradient B'. Here $L_{field} = \eta L$ where L is the lattice half period length;

$$L \approx 0.44\left(\frac{V}{1.0\times10^{6}}\right)^{1/4}\left(\frac{A}{q}\right)^{1/4}\left(\frac{a}{\eta B}\right)^{1/2} m \quad . \tag{6}$$

3. Driver Architectures

"Standard" Multiple Beam Architectures

The limitations on the line charge density per channel that can be transported using magnetic quadrupoles at low voltages have motivated multiple beam architectures with a large number (16–128) of electrostatically-focussed beams in the section below about 20-100 MeV, followed by a smaller number (4-32) of superconducting magnetic quadrupole channels. At pulse lengths longer than about one microsecond, the acceleration gradient is limited by the induction core material "packaging" to less than one MeV per meter (the limit on the gradient with the flux swing available from current magnetic materials, radially segmented core designs, etc., is generally taken to be around one volt-second/meter.) To accelerate the required total charge (~ one millicoulomb) to several GeV in a reasonable length, rapid longitudinal compression of the beam pulse is required as well as multiple beam channels.

As a specific reference case, consider the 4 MJ C_s^+ ion beam driver parameters presented in the Elise CDR [2]. To obtain the required one millicoulomb of charge, 64 "beamlets" are drawn from an ion source and accelerated in a multiple beam array to 100 MeV in an electrostatic quadrupole

(ESQ) focusing channel. The line charge density limitation of the ESQ given by Eq.(4), ~ 0.25 microcolombs/meter, results in a beam length of 63 meters and an initial pulse length of 37 microseconds (at the assumed gun voltage of 2 MeV). An induction core capable of 37 microseconds pulse length is truly massive, and it has a very low acceleration gradient (< 30 KV/meter). The beamlets are combined in groups of four at the 100 MeV point, to enter 16 magnetic quadrupole channels. At the point of entry into the magnetic channels, the resulting line charge density per beam of 1.0 μ coulombs/meter is much smaller than an optimized magnetic quadrupole channel could handle. Therefore, the beam length beyond this point is compressed as rapidly as possible to reduce the beam pulse duration and make a corresponding reduction in the induction core volume. At the output energy of 4 GeV, the pulse length is 7.5 meters (100 ns pulse duration) and the line charge density is 8.3 μ coulombs/meter per beam.

It would be nice if one could develop a more attractive architecture for the driver front end, even though the ultimate cost of a driver should still be dominated by the several hundred MeV to 4 GeV section. In addition, the recent emphasis on liquid wall reactor chambers and "non-vacuum" beam transport and focusing schemes motivate one to consider smaller numbers of output beams, to fully benefit from savings in beam transport and focusing systems costs and from simplifications in the reactor with a smaller number (and size) of reactor vessel penetrations.

As noted above, optimized quadrupole channels can carry much higher line charge densities than the reference design example utilized in the front end region. For example, at the 100 MeV point in the reference design, the line charge density in each quadrupole channel of about one microcoulomb per meter per beam is about 10x smaller than a 3-5 cm bore quadrupole channel with 8T pole face fields and $\eta = 0.25$ could carry. Combining a larger number of beams from the electrostatic quadrupole channels encounters the limitation in line charge density due to transverse emittance increases in the beam combining process.

A simple estimate will indicate the general limitations in line charge density from beam combining because of the space charge contributions to increases in the transverse emittance. If N beams are brought together to inject into a quadrupole channel, the inevitable voids and nonuniformities in the beam charge density distribution relative to a matched beam distribution function will result in some fraction "f" of the total radial potential variation across the beam, $\delta\phi = \lambda / 4\pi\varepsilon_0$ being converted into transverse kinetic energy, $Mv_t^2 / 2$. The increase in normalized transverse edge emittance from a process like this can be expressed as

$$\Delta\varepsilon_N^2 = \left\langle \frac{v_t^2}{c^2} a^2 \right\rangle \quad , \tag{7}$$

where "a" is the beam edge radius following beam combination. Therefore

$$\Delta\varepsilon_N = 3.8\times10^{-4} a \sqrt{f\frac{133}{A}} \sqrt{\frac{\lambda}{1.0\ \mu C/m}} \quad (\pi rad - meter) \tag{8}$$

is the space charge contribution to the emittance increase from beam combining. Detailed calculations of this process [3], with relatively optimistic assumptions about how well one can do with the beam combining optics, predict values for "f" of about 0.05. With this value of f, and for Cesium with a=3cm,

$$\Delta\varepsilon_N = 2.5\times10^{-6}\sqrt{\frac{\lambda}{1.0\ \mu C/m}} \quad (\pi\text{rad}-\text{meter}) \qquad (9)$$

The transverse normalized emittance requirement from final focusing considerations is about twice the value obtained from Eq. (9) with $\lambda = 1.0\ \mu C/m$. Therefore line charge densities just beyond the beam combining point cannot be much larger than what was assumed in the reference design discussed in the ILSE proposal. Indeed, beam combining at <u>any</u> point in the accelerator puts in a "choke point" that severely limits the line charge density.

<u>Solenoidal Front End</u>

As we have already indicated, the alternate architectures we would like to consider are those with a smaller number of beams sent to the target. The limitations in line charge density associated with beam combining motivate us to avoid it altogether, and keep the number of parallel beam channels constant.

A broad range of parameters are possible in principle with solenoidal transport; for example, a Cesium beam in a 5-10T superconducting solenoid magnet with a 30-50 cm radius can have a line charge density over 100μ coul / M according to Eq. (1). Avoiding excessive growth of transverse emittance in this situation, with a transverse potential drop across the beam of over 900KV, would be a real challenge (as would be the design of the injector and ion source). Indeed, the issue of maintaining the beam brightness in high current transport channels will ultimately determine the beam intensity limits for both the solenoidal and the magnetic quadrupole channels. For now, we will illustrate the solenoidal-based driver architecture possibilities with a "reference parameter set"; further study coupled with beam transport experiments will be needed to determine if these parameters are feasible, or are actually too conservative.

As reference parameters, consider a four beam system with the same total energy and charge as the previous case, namely one millicoulomb of singly charged Cesium ions accelerated to 4 GeV (see Fig. 1). Each beam pulse transported in the front end solenoidal transport system, with a field strength of 10T and edge radius of 10 cm, has a line charge density of 10.0μ coul / M and a length of 25 meters. With an injector voltage of 4MeV, the pulse duration is initially 10 microseconds. The selection of the transition point from solenoidal to magnetic quadrupole focusing is based on a comparison of line charge density limits in the two types of focusing channels (Eq 1 vs. Eq 5); 30 MeV is a reasonable choice on that basis with quadrupole parameters constrained by the aspect ratio L/a, where L is given by Eq. (6). With $\eta \le 0.5$, a value of Ba= 0.4 T-M insures adequate control of fringe field aberrations (e.g., 8T pole face field with a beam radius of 5 cm.).

At 30 MeV, the pulse duration is about 3.7 microseconds. Beyond this point, the beam length (in meters) is decreased as $1/\sqrt{V}$ according to the scaling of maximum line charge density (Eq 5). This strategy minimizes the pulse duration in the front end, which allows the highest possible gradient and minimizes the core material costs. At about 190 MeV, the pulse length has been reduced to 10 meters; beyond this point, the pulse length is kept constant as it is accelerated to 4 GeV.

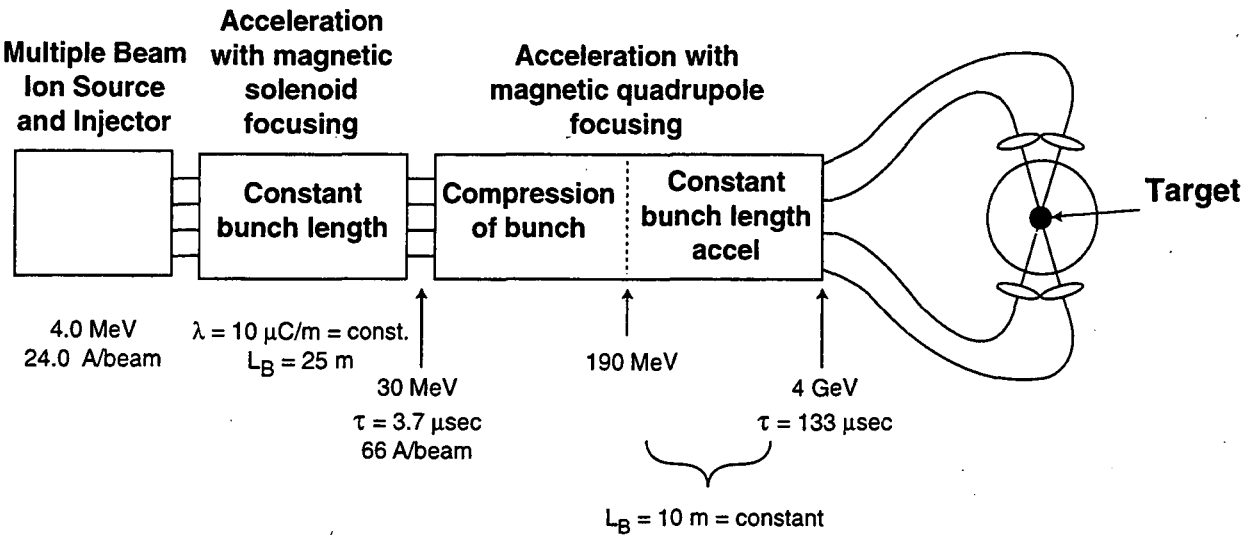

Figure 1. Solenoid-Based Four Beam Reference Design for Driver (Singly Charged Cesium)

The design of an injector that can produce a high brightness beam from a field-free anode and match it into the solenoidal field in Brillouin flow has not been done, and this is a critical part of the concept feasibility. Operation of the injector acceleration column at as high a voltage as possible helps to minimize the initial pulse length in the accelerator, and it may help the beam optics. With our 4 MeV choice, the injector output current (per beam) is about 25 amps, reasonable with an ion source of 20-25 mA/cm^2 (as achieved with smaller C_s^+ sources) and modest beam area compression ratios (~3-4).

The architecture for the "baseline" reference case has four beam transport channels inside of a common accelerator core, the "traditional" multiple beam configuration. With a relatively small number of beams, an alternate approach is to accelerate the pulses sequentially in a "burst mode" using a single transport channel. The pulses are brought to the target through different path lengths to have them arrive simultaneously. This approach requires burst mode pulse power systems and rapid core reset systems, which cost more and require development (but have high synergism with the advanced hydrodynamic radiography programs in DOE). This trades off with the reduction in beam transport system costs (factor of four) and the elimination of physics/technology issues involved in handling and accelerating multiple beams. Cost reductions would also accrue from the smaller core sizes possible with a smaller bore. Double pulsing has in fact been invoked in the past in reactor plant system studies to reduce the capital cost; a key question is whether a reduced electrical efficiency in the pulse power system offsets these potential advantages [4].

4. IRE Design Concepts

The heavy ion beam approach to Inertial Fusion Energy has always faced a very difficult programmatic problem: how to demonstrate key features of the concept in affordable research facility steps before proceeding to invest in driver-scale facilities. Lasers have basic advantages over high voltage accelerators in their development programmatics because the focusing of optical beams to high power densities can be demonstrated with "modest scale" modules that can be replicated "in parallel" to reach the multimegajoule pulse energies needed for ignition (exemplified by the beamlet module for NIF). Particle beams require relatively high voltage to be capable of focusing to a small

spot size, especially when they have the high peak currents and short pulses required for heating targets to ignition-relevant temperatures. Going to lower mass ions and lower beam voltages appears to be the best way to design a lower cost facility capable of meaningful scaled experiments on beam transport, acceleration, focusing, and target heating. In fact, this was the approach used in the past in conceptual designs of the so-called "High Temperature Experiment" (HTE) that had goals that were very similar to the IRE.

A detailed trade study and risk assessment would be required to optimize the design parameters of an IRE aimed at specific performance objectives within specified cost constraints. The objective of our discussion of the "strawman" IRE concept presented here is more modest: we want to make a plausible case that a sufficiently flexible and robust experimental facility based on solenoidal transport can be constructed at a cost of about $100-150M.

For a near term facility, the established technology of themionic potassium ion sources makes this ion a logical choice for a lighter mass IRE. (Flexibility of the facility to accelerate a range of ion masses with different sources is another desirable feature for IRE, but we will not examine this in the present paper.) Considerations of injector design, commercial capability for production of superconducting solenoidal magnets, and cost constraints related to beam pulse length motivated the following choice of "strawman" IRE parameters (as discussed further in the following paragraphs):

- Beam line charge density 5 microcoulombs/meter, beam radius 10 cm, solenoidal field 3.8T, injector voltage 4MeV, final beam energy 100 MeV, beam pulse length constant at 10 meters (FWHM, ~12 meters total length including the ends).

- These parameters imply an initial beam pulse duration out of the injector of 2.3 microseconds (FWHM), an initial beam current of 22A, a final beam pulse duration of 0.45 microseconds, a final beam current of 110A, and an output pulse energy of 5 KJ's.

Injector

The main issues in the injector design are the optics design capable of generating the required low emittance, uniform current density beam, and the maximum voltage stresses allowed on electrodes and insulators.

The most relevant experience base regarding the optics design of high brightness, high current heavy ion beams is that of intense nonrelativistic electron beams for microwave devices and electron accelerators. (The radial defocusing of high current relativistic electron beams in the gun region is significantly reduced by the self magnetic fields, making their optics design less relevant). Electron guns for high power klystrons have perveances around 2 micropervs, but their current densities are relatively nonuniform. Electron gun design experience suggests that electron gun perveances need to be below about one microperv to produce adequate current density uniformity following beam injection into the focusing solenoidal field. One rule of thumb for generating uniform current densities is a ratio of less than 1/3 in the cathode radius "a" to (effective) acceleration gap distance "d" in a planar Child-Langmuir law; this rule of thumb corresponds to a perveance of 0.8 micropervs.

Our IRE parameter choice corresponds to a heavy ion (potassium) gun perveance of 2.75 nanopervs; the equivalent nonrelativistic electron gun perveance, scaling with the square root of the mass, is 0.74 micropervs, which is within the experience-based gun optics criteria discussed above. Note that for the driver parameters discussed in the previous section, we have assumed that these optics criteria can be exceeded by a factor of two (or that higher voltage injectors will be feasible on

these longer development time scales). For IRE, a somewhat more conservative parameter goal seems appropriate, at least until detailed gun design studies have been completed.

At an emission current density of 20 mA/cm^2, at the upper end of what has been demonstrated to date with these sources, an ion source diameter of 37.5 cm (15 inches) is required. This is about twice the diameter of the ion sources currently in use in the LBNL injector test stand (and these also operate at much smaller current densities). The mean gun voltage stress, V/d, is of order 60-70 kV/cm with these source dimensions.

We believe these "strawman" injector parameters are plausible extrapolations of current technology, but it is clear that the injector design and development is the critical path item required to finalize the IRE parameters. More conservative parameters, like 2-3 microcoulombs/meter, would be the fallback parameter choice if the "strawman" injector parameters prove too difficult to achieve on the required time frame.

Superconducting Solenoids

As mentioned in the introduction, a significant industrial capability exists in superconducting solenoid manufacturing for applications like NMR and MRI. Wire wound superconducting solenoids are much simpler to construct than the superconducting dipole and quadrupole magnets used extensively in conventional high energy particle physics accelerators, of course, and their procurement on a fixed price basis should be relatively straightforward.

At this point, in the absence of engineering designs or detailed specs on field quality, etc., a rough order of magnitude cost estimate is all we are after. Discussions with several superconducting magnet specialists with knowledge of the relevant industrial production processes lead to the following "top down" cost SWAGS.

The unit package envisioned for our strawman parameter set would consist of a 4T, 30 cm. diameter bore coil, about one meter long, with a radial build about 1.5 cm. and a 2-3 cm. thick heat shield. Note that the wire volume per meter of length, scaling as Ba, is very close to a "standard" MRI machine with 1.5T field and a one meter bore. Complete magnet systems for these machines, including power supplies, controls, etc., are in the general ballpark of $150-300K with a magnet length of 1.5 meters. On a per meter basis, using simple Ba scaling, this translates into $80-160K per solenoid for the strawman system. Of course, the cryostat would be an entirely new design, and many other features of the MRI machine magnets operating with persistent currents and highly uniform fields should be simplified in our case. For example, an independent SWAG by a small vendor with experience in NMR coil production put the costs of our one meter unit in the $50-75K range.

If we take a unit magnet cost of $50-100K per meter and a machine length of 200 meters, corresponding to an average gradient of 0.5 MeV/meter and 100 MeV output, the total transport magnet cost would be in the $10-20M range.

Accelerator

The induction accelerator cores need to supply a voltage pulse about 2.7 microseconds long at the front end, decreasing at the higher energy end according to $1/V^{1/2}$ in the baseline acceleration mode with the beam pulse length (line charge density) held constant. Since the IRE facility should be as flexible as possible in its capability to study a wide variety of acceleration schedules and beam

transport physics issues, and a large number of different core designs would be costly, the machine would probably be built using only a few core types. For example, the first 4 MeV of accelerator (to 8 MeV) could use the 2.7 microsecond cores, the section from 8 to 30 MeV designed for 2 microseconds pulse length, and the final section designed for 1 microsecond pulse length. The pulsers will need to have waveform control "knobs" for things like compensating the axial expansion forces from the space charge fields of the beam, maintaining a flat energy profile, and studying various axial compression schedules.

The major new feature in this IRE concept is the integration of superconducting solenoids inside the induction cores. Otherwise, the components are generally similar to the "long pulse" induction machines built in the past (NBS, Astron), or (more recently) the electron machines designed for applications like radiography for hydrotests in the nuclear weapons program. A recent study of a 2.2 microsecond, 20 MeV, 4 KA electron accelerator for the second axis of DARHT [5] provides a very useful reference point for a ballpark estimate of the cost of our "strawman" IRE. A rough estimate of the "DARHT-2" machine, with no contingency or conventional facilities, is about $36M ($23M is the cost of the hardware). The DARHT-2 design provides 8KA total current to the cell, half into the beam; our beam loading is negligible compared to this. On the other hand, the IRE pulsers will need to be much more flexible and capable in waveform control, so the pulse power cost (per volt-sec provided) might still end up roughly comparable. The 10 inch bore of the DARHT-2 beam tube design would also need to be increased somewhat to accommodate the 10 cm heavy ion beam radius. If we simply scale the machine costs by the volt-secs of the total voltage waveform provided, and use the "segmentation" into different pulselengths outlined above for the IRE, we have a cost for the 100 MeV IRE of 3.3 times the 20 MeV DARHT-2 or about $120M (without the superconducting focus magnets). Including the magnets, the overall cost on this crude scaling basis would be a little less than $150M.

Incidentally, the DARHT-2 injector is a 3 MeV Marx largely modeled after the LBNL IFE injector, so these costs should be very similar. A more refined scaling subtracting out the $4.5M injector and other fixed cost items before applying the volt-secs multiplier reduces the above SWAG by $20-30M.

More refined calculations and optimizations would undoubtedly provide a basis for lowering this SWAG on the accelerator construction, but the total project cost would ultimately have to include a number of items that we left out. We have not, for example, included anything to cover a transport section for beam compression, or facilities for final focus and target heating studies. The only conclusion we would draw from these general considerations is that one should be able to build a machine on the general scale of our 100MeV IRE strawman for less than $150M; a more conservative projection would indicate a machine of 50-75MeV fitting within this cost envelope. Improving on this SWAG will require a clear definition of the scope of what is to be included in the facility construction budget, as opposed to the items that would be covered later as part of the experimental operations budget, and a more complete conceptual design for cost estimating.

5. Solenoidal Transport Physics

Since solenoidal transport at low energy is the distinctive feature of the driver and IRE concepts described here, a derivation of basic dynamical effects has been included. Most of this material does not appear to have anything really new in it, but neither has it been previously gathered in a form convenient for the fusion driver application. The books by Lawson [6], Davidson [7] and Reiser [8] are useful general resources on this subject.

In the following subsections we derive the axisymmetric envelope equation and single particle equation and apply them to the case of Brillouin flow. Matched envelope solutions and oscillations

of the beam radius are treated, including the interesting case of a beam subject to a periodic variation of B_z. A brief treatment of aberrations of a cold beam, using a fluid model is also included.

5.1 Envelope equation for an axisymmetric beam

A useful approximate equation governing the z-dependent beam edge radius is derived from the transverse equations of motion for the ions:

$$\frac{d^2x}{dt^2} = \frac{qe}{M}\left(E_x + \frac{dy}{dt}B_z - \frac{dz}{dt}B_y\right) \quad , \tag{10a}$$

$$\frac{d^2y}{dt^2} = \frac{qe}{M}\left(E_y + \frac{dz}{dt}B_x - \frac{dx}{dt}B_z\right) \quad . \tag{10b}$$

We follow the motion of a thin disk of ions as it moves forward at velocity v_z. Either time (t) or longitudinal position (z) can be used as an independent variable, but z is more convenient since fields from electrodes and coils are specified as functions of z. We consider v_z to be a known function of z for the disk and replace the time derivative

$$\frac{d}{dt} \rightarrow v_z(z)\frac{d}{dz} \equiv v_z \quad . \text{ "prime"} \tag{11}$$

For the field expressions only the lowest order terms in x and y are retained (a higher order analysis is given in section 5.4):

$$B_z \cong B_z(z) \quad , \tag{12a}$$

$$B_r = -\frac{1}{2}\frac{dB_z}{dz}r \quad , \tag{12b}$$

$$E_z = E_z(z) \quad , \tag{12c}$$

$$E_r = \left(\frac{\lambda}{2\pi\varepsilon_0 a^2} - \frac{1}{2}\frac{dE_z}{dz}\right)r \quad . \tag{12d}$$

Here $\lambda(z)$ is the beam's line charge density and a(z) is the edge radius. The first term on the right in equation (12d) is clearly correct only for a flat top charge profile. However, an envelope equation derived directly using rms quantities yields an equivalent radial electric field in an averaged sense. We have from equations (10-12):

$$v_z\frac{d}{dz}v_z\frac{dx}{dz} = \frac{qe}{M}\left[\left(\frac{\lambda}{2\pi\varepsilon_0 a^2} - \frac{1}{2}\frac{dE_z}{dz}\right)x + v_z B_z\frac{dy}{dz} + \frac{v_z}{2}\frac{dB_z}{dz}y\right], \tag{13a}$$

$$v_z\frac{d}{dz}v_z\frac{dy}{dz} = \frac{qe}{M}\left[\left(\frac{\lambda}{2\pi\varepsilon_0 a^2} - \frac{1}{2}\frac{dE_z}{dz}\right)y - v_z B_z\frac{dx}{dz} - \frac{v_z}{2}\frac{dB_z}{dz}x\right]. \tag{13b}$$

These transverse equations are supplemented by the longitudinal dynamical equation

$$v_z \frac{dv_z}{dz} = \frac{dv_z}{dt} = \frac{qe}{M} E_z \quad . \tag{14}$$

Transformation to a rotating frame is now made:

$$x = X\cos\phi - Y\sin\phi \quad , \tag{15a}$$

$$y = X\sin\phi + Y\cos\phi \quad . \tag{15b}$$

Defining the cyclotron frequency

$$k_c(z) = \frac{qeB_z}{Mv_z} \quad , \tag{16}$$

The choice

$$\phi(z) = -\frac{1}{2}\int_0^z dz' k_c(z') \tag{17}$$

decouples the x-y motion, giving

$$X'' + \frac{v_z'}{v_z} X' = -\frac{k_c^2}{4} X - \frac{v_z^{2'}}{4v_z^2} X + \frac{Q}{a^2} X \quad , \tag{17a}$$

$$Y'' + \frac{v_z'}{v_z} Y' = -\frac{k_c^2}{4} Y - \frac{v_z^{2'}}{4v_z^2} Y + \frac{Q}{a^2} Y \quad . \tag{17b}$$

Here we have used the dimensionless perveance of Lawson (non-relativistic limit)

$$Q = \frac{qe\lambda}{2\pi\varepsilon_0 M v_z^2} = \frac{\lambda(z)}{4\pi\varepsilon_0 V(z)} \quad , \tag{18}$$

with V(z) defined to be the "cumulative voltage" felt by the beam:

$$V(z) \equiv \frac{Mv_z^2}{2qe} \quad . \tag{19}$$

Because the system is axisymmetric, the canonical angular momentum of an ion is conserved; in the laboratory frame we define (in lowest order in r)

$$\ell = \frac{P_\theta}{M} = r\left(v_\theta + \frac{qe}{M}\frac{B_z r}{2}\right) = \text{ constant} \quad . \tag{20}$$

This may be written as

$$\ell = v_z\left[(xy' - yx') + \frac{k_c r^2}{2}\right] \quad . \tag{21}$$

Substitution of rotated variables from equations (15a,b) yields

$$\ell = v_z(XY' - YX') \quad . \tag{22}$$

The conservation of ℓ may be readily demonstrated from equations (17a,b).

To obtain an envelope equation we define some averages over the beam slice:

$$R^2 = \overline{r^2} = \overline{X^2} + \overline{Y^2} = \frac{a^2}{2} \quad , \tag{23a}$$

$$U^2 = \overline{X'^2} + \overline{Y'^2} \tag{23b}$$

$$L = \frac{\bar{\ell}}{v_z} \quad . \tag{23c}$$

Two useful moments of equations (17a,b), relating R and U are

$$\frac{R^{2''}}{2} - U^2 + \frac{v_z'}{v_z}\frac{R^{2'}}{2} = \left(-\frac{k_c^2}{4} - \frac{v_z^{2''}}{4v_z^2} + \frac{Q}{a^2}\right)R^2 \quad , \tag{24}$$

$$\frac{U^{2'}}{2} + \frac{v_z'}{v_z}U^2 = \left(-\frac{k_c^2}{4} - \frac{v_z^{2''}}{4v_z^2} + \frac{Q}{a^2}\right)\frac{R^{2'}}{2} \quad . \tag{25}$$

We also have from equations (22) and (23c)

$$(Lv_z)' = 0 \quad . \tag{26}$$

A mean-squared emittance is defined as

$$E^2 = R^2\left[U^2 - R'^2 - \frac{L^2}{R^2}\right] \quad . \tag{27}$$

Then equations (24)-(26) yield, after some manipulations

$$v_z^2 E^2 = \text{constant} \quad . \tag{28}$$

Hence the assumed linear approximation of the dynamical equations conserves an appropriately defined normalized emittance, as might be expected. The emittance E, as defined in equation (27). contains only the thermal and aberration parts of ion transverse velocity.

Using equation (27) to eliminate U^2 from equation (24) in favor of E^2 we get

$$R'' + \frac{v_z'}{v_z} R' = \frac{E^2 + L^2}{R^3} - \frac{k_c^2}{4} R - \frac{v_z''}{4v_z^2} + \frac{Q}{a^2} R \quad . \tag{29}$$

Noting that R and E are rms quantities, we may obtain an envelope equation for edge-defined quantities (a, ε) by the substitutions $R = a/\sqrt{2}$, $E = \varepsilon/2$:

$$a'' + \frac{v_z'}{v_z} a' = \frac{\varepsilon^2 + 4L^2}{a^3} - \frac{k_c^2}{4} a - \frac{v_z''}{4v_z^2} a + \frac{Q}{a} \quad . \tag{30}$$

Another form of the envelope equation is obtained by the substitution $a(z) = b(z)/\sqrt{\beta}$, where $\beta = v_z/c$:

$$b'' = \frac{(\varepsilon\beta)^2}{b^3} + \frac{(2L\beta)^2}{b^3} - \left(\frac{k_c}{2}\right)^2 b + \frac{(Q\beta)}{b} - \frac{3}{4}\left(\frac{\beta'}{\beta}\right)^2 b \quad . \tag{31}$$

Although b(z) differs from a(z) by the inconvenient factor $\sqrt{\beta(z)}$, the conserved quantities $\varepsilon\beta$ and $L\beta$ now appear explicitly in the envelope equation and terms involving β'' and b' are removed. Equation (31) may be applied to source and extraction problems as well as envelope dynamics during downstream transport, acceleration and focusing.

5.2 Particle Orbits in a Uniform Solenoid

Brillouin flow is the constant-radius beam equilibrium with the maximum possible charge density that can be transported in a uniform solenoid field with given edge radius. In the elementary model of this beam equilibrium, the ions (injected into the field from a field free ion source) rotate about the axis at a constant angular velocity of $-\omega_c/2$, where

$$\omega_c = qeB_z / M \quad . \tag{32}$$

In this simple model, the beam density ρ is uniform, and the axial velocity of the ions in a monoenergetic beam turns out to be independent of radius position r. Ions near the axis are retarded from the potential depression; this reduction in axial velocity is exactly equal to the reduction at large radius from the increasing azimuthal velocity.

This ideal can only be approximated in the real world, of course. While particle simulation codes are needed for quantitative evaluations of effects like finite beam source temperature (emittance), mismatches, nonuniform densities, etc., it is useful to first gain physical insight from various simple models. Here we look at particle orbits in a uniform density beam to see what the orbits are

like when the magnetic field is somewhat larger than the Brillouin value and/or the ions have a finite emittance. One might expect that the ions would have only a small deviation away from the constant-radius rotation of the elementary model, but this is only true for a limited time, as we now show.

In order to make clear a connection with plasma physics and generally stimulate the reader, variables of time (t) and frequency (ω_c, ω_p) are used in this subsection instead of z, k_c and Q as in 5.1. Cartesian coordinates are useful when the charge density is approximately uniform, and the solenoidal magnetic field can be described in the paraxial approximation. With these approximations, the transverse equations of motion can be written as

$$\frac{d^2x}{dt^2} = \frac{\omega_p^2}{2}x + \frac{dy}{dt}\omega_c + \frac{y}{2}\frac{\partial\omega_c}{\partial z}\frac{dz}{dt} \quad , \tag{33a}$$

$$\frac{d^2y}{dt^2} = \frac{\omega_p^2}{2}y - \frac{dx}{dt}\omega_c - \frac{x}{2}\frac{\partial\omega_c}{\partial z}\frac{dz}{dt} \quad , \tag{33b}$$

where

$$\omega_p^2 = \frac{qe\rho}{\varepsilon_0 M} \tag{34}$$

is the beam plasma frequency.

Multiplying Eq. 33(b) by x and subtracting y times Eq.33(a), we find the conservation of canonical angular momentum in the form

$$\ell = x\frac{dy}{dt} - y\frac{dx}{dt} + \frac{\omega_c}{2}\left(x^2+y^2\right) = \text{constant} \quad . \tag{35}$$

If the ions are born in a field-free region with zero transverse velocity, then $\ell=0$.

In a uniform magnetic field, the solutions to Equations 33a and 33b can be written as a linear superposition of two circular motions,

$$x(t) = A\cos\left(\omega_1 t+\psi_1\right) + B\cos\left(\omega_2 t+\psi_2\right) \quad , \tag{36a}$$

$$y(t) = -A\sin\left(\omega_1 t+\psi_1\right) - B\sin\left(\omega_2 t+\psi_2\right) \quad , \tag{36b}$$

where

$$\omega_1 = \frac{\omega_c}{2} + \omega,\ \omega_2 = \frac{\omega_c}{2} - \omega \quad , \tag{37a}$$

$$\omega = \left[\frac{\omega_c^2}{4} - \frac{\omega_p^2}{2}\right]^{1/2} \quad . \tag{37b}$$

The Brillouin flow condition is $\omega = 0$. From Eq.(35), we have in general

$$\ell = \omega\left(B^2 - A^2\right) \quad . \tag{38}$$

Setting $\omega = 0$ in equation (37a), we recover circular motion at the frequency $-\omega_c/2$ and a constant (arbitrary) radius, as predicted by the elementary model. If the field is reduced below the Brillouin limit, equation (37b) clearly shows that there is no stable orbit unless ρ is also decreased.

If the field is increased above the Brillouin limit, the particle motion is no longer at a constant radius. In this case we find

$$r^2 = x^2 + y^2 = A^2 + B^2 + 2AB\cos\left(2\omega t + \psi\right) \quad , \tag{39}$$

and the particles move between

$$r_{max} = A + B \quad , \tag{40}$$

and

$$r_{min} = |A - B| \tag{41}$$

with period π/ω. Note that the cannonical angular momentum can be written

$$\ell = \pm \omega r_{max} r_{min} \quad . \tag{42}$$

If the ions are injected cold from a field-free region, then $\ell = 0$ and $r_{min} = 0$, and this simple constant density model predicts they will (eventually) pass through the axis when $\omega \neq 0$.

It is interesting to estimate from these orbit solutions how much the magnetic field must be increased above the Brillouin value to contain a set of particles of finite emittance. A finite emittance beam will have particles with a distribution of ℓ values, of order

$$|\ell| \approx \varepsilon_N c \quad . \tag{43}$$

where ε_N is the normalized transverse edge emittance (without a π). From Eq. (42), if $r_{max} r_{min}$ is of order a^2, we have

$$\Delta = \frac{\omega}{\omega_c/2} \approx \frac{2\varepsilon_N c}{\omega_c a^2} \quad . \tag{44}$$

This requirement is consistent with the envelope equation, Eq (30) of 5.1.

As an example, consider $B = 3.8T$, $a = 10cm$, $A = 39$, and $\varepsilon_N = 5\times10^{-6}\,m - r$ (the IRE point design); Eq. (44) yields

$$\Delta \approx 3.2\times10^{-2} \tag{45}$$

and an increase in the solenoidal field above the Brillouin value by only

$$\frac{\Delta B}{B} \approx \Delta^2/2 \approx 5\times 10^{-4} \tag{46}$$

is needed to maintain equilibrium at the same ρ and a.

5.3 Applications of the Envelope Equation

Here we examine, in a rudimentary fashion, the dynamics of a beam transported in a solenoid without acceleration and having zero average canonical angular momentum. The envelope equation is then:

$$\frac{d^2a}{dz^2} = -\frac{k_c{}^2(z)}{4}\,a + \frac{\varepsilon^2}{a^3} + \frac{Q}{a} \quad , \tag{47}$$

and the single particle equation of motion in a reference frame rotating at the rate $d\phi/dz = -k_c/2$ is:

$$\frac{d^2x}{dz^2} = -\frac{k_c^2}{4}\,x + \frac{Q}{a^2}\,x \quad . \tag{48}$$

Case 1: Matched Beam, Constant $k_c(z)$

Setting $k_c = k_{c_0}$, the matched beam radius has constant value a_0, satisfying

$$0 = -\frac{k_{c_0}{}^2}{4}a_0 + \frac{\varepsilon^2}{a_0{}^3} + \frac{Q}{a_0} \quad . \tag{49}$$

This is quadratic in a_0^2, so we get

$$a_0{}^2 = \frac{2Q}{k_{c_0}{}^2} + \sqrt{\left(\frac{2Q}{k_{c_0}{}^2}\right)^2 + \frac{4\varepsilon^2}{k_{c_0}{}^2}} \quad . \tag{50}$$

It is useful to define the particle trajectory "tunes": σ_0 = "undepressed tune", and σ = "depressed tune", corresponding respectively to $Q = 0$ and Q finite. Let P denote a periodicity length of the solenoid, which is arbitrary for the case of constant k_c. Then σ_0 is the particle oscillation phase advance per period with $Q = 0$:

$$\sigma_0 = \frac{k_{c_0}\,P}{2} \quad , \tag{51}$$

and σ is the phase advance reduced by the space charge force represented by finite Q:

$$\sigma = \sqrt{\frac{k_{c_0}^2}{4} - \frac{Q}{a_0^2}}\ P \quad . \tag{52}$$

From equations (49) - (52) we are able to relate emittance and perveance to the tunes:

$$\varepsilon = \frac{\sigma a_0^2}{P} \quad , \tag{53}$$

$$Q = \left(\sigma_0^2 - \sigma^2\right) \frac{a_0^2}{P^2} \quad . \tag{54}$$

In the limit $\sigma \sim \varepsilon = 0$, equation (49) gives the Brilloiun flow limit

$$Q = \frac{k_{c_0}^2 a_0^2}{4} \quad , \tag{55}$$

from which we obtain the transportable line charge density

$$\lambda \equiv \left(4\pi\varepsilon_0 \frac{Mv^2}{2qe}\right) Q = \left(4\pi\varepsilon_0 \frac{Mv^2}{2qe}\right) \left(\frac{qe\, B_z}{Mv}\right)^2 \frac{a_0^2}{4}$$

$$= \frac{\pi\varepsilon_0}{2} \frac{qe}{M} B_z^2 a_0^2$$

$$= \left(10.0 \frac{\mu C}{m}\right) \left(\frac{133q}{A}\right) \left(\frac{B_z}{10T}\right)^2 \left(\frac{a_0}{10cm}\right)^2 \quad . \tag{56}$$

Case 2 : Small Amplitude Oscillation For Constant k_c

We set $a(z) = a_0 + \delta a(z)$ with $\delta a << a_0$. Then equation (47) may be linearized:

$$\frac{d^2\delta a}{dz^2} = -\frac{k_{c_0}^2}{4} \delta a - \frac{3\varepsilon^2}{a_0^4} \delta a - \frac{Q}{a_0^2} \delta a \quad , \tag{57}$$

$$= -\frac{k_{c_0}^2}{2} \left(1 + \frac{\sigma^2}{\sigma_0}\right) \delta a \quad ,$$

where we have used the equilibrium relations to eliminate ε, a_0, and Q.

The natural oscillation frequency is therefore:

$$\Omega = \frac{k_{c_0}}{\sqrt{2}} \sqrt{1 + \frac{\sigma^2}{{\sigma_0}^2}} \quad . \tag{58}$$

For $\sigma \rightarrow 0$ (Brillouin flow) the natural oscillation frequency is denoted $\Omega_0 = k_{c_0}/\sqrt{2}$, which is larger than the Larmour frequency by $\sqrt{2}$.

Case 3: Sinusoidal Variation of $k_c(z)$ – Matched Envelope, Brillouin Flow

For periodic $k_c(z)$ there exists, in general, a solution of the envelope equation with the same period. This solution is "ideal" in the sense that it is as close to constant radius as can be arranged. We set:

$$k_c(z) = k_{c_0} (1 + \varepsilon \cos Kz) \quad , \tag{59}$$

where ε is a small dimensionless parameter (not the emittance, which is now equal to zero) and the period length P now has the definite value $P = 2\pi/K$. The matched envelope radius a(z) is the solution of the envelope equation with period P:

$$\frac{d^2a}{dz^2} = - \frac{{k_{c_0}}^2}{4} (1 + \varepsilon \cos Kz)^2 \, a + \frac{Q}{a} \quad , \tag{60}$$

$$a(z + P) = a(z) \quad .$$

It is convenient to write eqn. (60) in the following form:

$$a = a_0 (1 + f(z)) \quad , \tag{61}$$

$$\frac{d^2f}{dz^2} = - \frac{{\Omega_0}^2}{2} \left[(1 + \varepsilon \cos Kz)^2 (1 + f) - \frac{1}{1 + f} \right] \quad , \tag{62}$$

where $\Omega_0 = k_{c_0}/\sqrt{2}$ is the natural small amplitude oscillation frequency in the limit $\varepsilon \rightarrow 0$ and $Q = \Omega_0^2 a_0^2/2$. The form of the matched function $f = f_m(z)$ can be written as an expansion in powers of ε.

$$f_m = \varepsilon A \cos Kz + \varepsilon^2 B + \varepsilon^2 C \cos 2Kz + \ldots \quad . \tag{63}$$

Inserting this form into equation (62) and equating the coefficients of terms of the form $\varepsilon^n \cos mKz$, we get:

$$A = \frac{1}{\alpha - 1} \quad , \tag{64}$$

$$B = \left(\frac{A^2}{4} - \frac{A}{2} - \frac{1}{4} \right) \quad , \tag{65}$$

$$C = - \frac{B}{(4\alpha - 1)} \quad , \tag{66}$$

where $\alpha \equiv (K/\Omega_0)^2$. The assumed expansion in $\varepsilon^n \cos (m\,Kz)$ is seen to blow up when $\alpha = 1$, 1/4, 1/9, etc, i.e., when the smooth limit wave frequency Ω_0 is an integer multiple of the solenoid frequency K. Generally a transport channel would be designed to operate with α well above unity for this reason. This condition means that the cyclotron period $\left(2\pi/k_{c_0}\right)$ should be greater than $P/\sqrt{2}$. In fact a condition for stability (to be derived below), suggests that the cyclotron period should be greater than $\sqrt{2}\ P$ to avoid unstable growth near a "half integer resonance". Maximum and minimum values of f_m for $\varepsilon = 0.2$ are given in a table at the end of this section.

Case 4: Stability of the Matched Envelope

Equation (62) may be linearized to treat a small amplitude axisymmetric perturbation away from the matched function f_m:

$$f = f_m + \delta f \quad , \tag{67}$$

where $\delta f << f_m$. Then the equation for δf is:

$$\frac{d^2}{dz^2}\,\delta f = - \frac{\Omega_0^2}{2} \left[(1 + \varepsilon \cos Kz)^2\, \delta f + \frac{1}{(1+f_m)^2}\, \delta f \right] \tag{68}$$

$$= - \Omega_0^2 \left[1 + \varepsilon (1 - A) \cos Kz + \varepsilon^2 \left(\frac{1}{4} - B + \frac{3}{4} A^2 \right) \right.$$

$$\left. + \varepsilon^2 \left(\frac{1}{4} - C + \frac{3}{4} A^2 \right) \cos 2\,Kz + 0\left(\varepsilon^3\right) \right] \delta f \quad . \tag{68a}$$

Equation (68) is readily solved by a simple numerical technique. It is also analytically solvable in its approximate form (68a). We do both. The analytical approach is presented in moderate detail here to bring out the physics of the stop band associated with a half integer resonance.

Just as for f_m (z), we solve for δf through order ε^2, so terms of order ε^3 or higher are consistently dropped. The term on the rhs of equation (68a) proportional to $\varepsilon^2 \cos(2\,Kz)$ cannot affect the mode frequency or growth rate through order ε^2, so it may be dropped. However, the term proportional to $\varepsilon^2\left(\frac{1}{4} - B + \frac{3}{4} A^2\right)$ does shift the basic wave frequency in order ε^2. We therefore define:

$$\Omega^2 = \Omega_0{}^2 \left[1 + \varepsilon^2 \left(\tfrac{1}{4} - B + \tfrac{3}{4} A^2\right)\right] \quad , \tag{69}$$

and replace equation (68a) with the simpler form:

$$\frac{d^2\,\delta f}{dz^2} + \Omega^2\,\delta f = -\,\Omega_0^2\,\varepsilon\,(1-A)\,(\cos Kz)\,\delta f \quad . \tag{70}$$

The stability of the mode is determined from the eigenvalues (λ) of the transfer matrix for period $P = 2\pi/K$ associated with equation (70):

$$\begin{bmatrix} \delta f\,(P) \\ \delta f'(P) \end{bmatrix} = \begin{bmatrix} M_{11} & M_{12} \\ M_{21} & M_{22} \end{bmatrix} \begin{bmatrix} \delta f\,(0) \\ \delta f'(0) \end{bmatrix} \quad . \tag{71}$$

Due to the symmetry of $k_c(z)$ around $z = 0$, it can be shown that $M_{22} = M_{11}$. Exploiting the symplectic condition $\| M \| = 1$, the eigenvalues (λ) are found to satisfy:

$$0 = \| M - I\lambda \| = 1 - 2\,M_{11}\,\lambda + \lambda^2 \quad . \tag{72}$$

This is solved by:

$$\lambda = M_{11} \pm \sqrt{M_{11}{}^2 - 1} \quad . \tag{73}$$

For $| M_{11} | < 1$, we set:

$$M_{11} \equiv \cos\phi \quad , \tag{74}$$

$$\lambda = \cos\phi \pm i \sin\phi = e^{\pm i\phi} \quad , \tag{75}$$

i.e., we get stable oscillations with phase advance per period (ϕ). For $| M_{11} | > 1$ the phase advance locks at a multiple of 180° and λ has two real values, one of which has magnitude greater than unity. This is the growth factor per period of an unstable mode.

The problem of finding ϕ or λ is therefore reduced to that of evaluating M_{11} with sufficient accuracy, in this case through terms of order ε^2. This is readily done by noting that M_{11} is

identical with the solution $\delta f(P)$ for initial conditions $\delta f(0) = 1.0$, $\delta f'(0) = 0$. In lowest order in ε we have $\delta f = \cos \Omega z$; this may be inserted on the rhs of equation (70) and an improved solution obtained by integration. This procedure is repeated, keeping terms through order ε^2 and observing the initial condition $\delta f'(0) = 0$. Then we calculate M_{11}, and λ is determined from equation (72). Sparing the reader the details of this iterative calculation, the final result is:

$$M_{11} \cong \cos \Omega P - \frac{\varepsilon^2 \Omega_0^4 P (1-A)^2}{8\Omega} \left[\frac{1}{(K+\Omega)^2 - \Omega^2} + \frac{1}{(K-\Omega)^2 - \Omega^2} \right] \sin \Omega P$$

$$\approx \cos\left(\frac{2\pi\,\Omega}{\sqrt{\alpha}\,\Omega_0}\right) - \frac{\varepsilon^2}{8}\left(\frac{\alpha-2}{\alpha-1}\right)^2 \frac{2\pi}{\sqrt{\alpha}} \frac{\Omega_0}{\Omega} \sin\left(\frac{2\pi}{\sqrt{\alpha}} \frac{\Omega}{\Omega_0}\right) \cdot$$

$$\cdot \left[\frac{1}{\left(\sqrt{\alpha} + \frac{\Omega}{\Omega_0}\right)^2 - \left(\frac{\Omega}{\Omega_0}\right)^2} + \frac{1}{\left(\sqrt{\alpha} - \frac{\Omega}{\Omega_0}\right)^2 - \left(\frac{\Omega}{\Omega_0}\right)^2} \right] , \tag{76}$$

with

$$\frac{\Omega}{\Omega_0} = \left[1 + \frac{\varepsilon^2}{2} \frac{\alpha^2 - \alpha + 1}{(\alpha-1)^2} \right]^{1/2} . \tag{77}$$

Values of phase advance ϕ or growth factor λ are tabulated below along with the values of $1 + f_m$ at 0 and P/2 for $\varepsilon = 0.2$ and various values of α. The expected stable behavior for large α is evident, with the value $\phi = 180°$ approached at $\alpha \approx 4.4$. An unstable stop band occupies the range $\alpha \approx 4.4 - 3.85$, i.e., close to the half integer resonance $\Omega_0 \approx K/2$. Decreasing α below 3.85 again yields stable oscillations with $\phi > 180°$. Note the relatively low maximum growth factor ≈ 1.11 in the stop band and the excellent agreement between analytical and numerical results.

An interesting behavior of the matched envelope $a = a_0[1 + f_m(z)]$ emerges in the band $1 < \alpha < 2$. Very large maximum amplitudes appear, with the minimum of $a(z)$ approaching close to zero, making computations difficult. This unexpected behavior appears to be associated with the existence of a finite amplitude oscillation of the beam radius with frequency in the range $\left(1.0 \text{ to } \sqrt{2}\right) \Omega_0$ when $\varepsilon = 0$.

STUDY $\varepsilon = 0.2$

Numerical				Analytical		
α	$\frac{a(0)}{a_0}$	$\frac{a(P/2)}{a_0}$	ϕ λ	$\frac{a(0)}{a_0}$	$\frac{a(P/2)}{a_0}$	ϕ λ
16.00	1.00228	.97587	91.02^0	1.00222	.97556	91.02
8.00	1.01631	.95965	128.99^0	1.01633	.95918	128.99^0
6.00	1.02695	.94754	149.27^0	1.02699	.94699	149.27
4.40	1.04471	.92767	178.40^0	1.04471	.92706	178.90^0
4.35	1.04554	.92674	-1.0535	1.04554	.92614	-1.0567
4.25	1.04730	.92481	-1.0909	1.04728	.92420	-1.0941
4.15	1.04916	.92275	-1.1055	1.04913	.92214	-1.1082
4.10	1.05014	.92167	-1.1062	1.05011	.92107	-1.1090
4.00	1.05220	.91940	-1.0940	1.05215	.91881	-1.0977
3.90	1.05441	.91698	-1.0519	1.05433	.91640	-1.0586
3.85	1.05557	.91571	182.31^0	1.05549	.91513	181.71^0
3.00	1.08470	.88432	211.16^0	1.08409	.88409	211.00^0
2.00	1.19125	.77679	262.84^0	1.18286	.78286	262.08^0
1.50	1.59683	.44930	334.38^0	1.3920	.59200	312.95^0
No useful solution found near $\phi = 360^0$						
1.00	.11369	2.49777	423.99^0	Divergent		
.75	.37848	1.80152	435.41^0	.31500	1.91500	445.70^0
.50	.60955	1.38640	512.72^0	.60000	1.40000	514.88^0

Table 1. For various values of α and $\varepsilon = 0.2$ we compute a/a_0 at $z = 0$ and $P/2$, phase advance (ϕ) per period (P), or unstable growth factor λ per period. Numerical results were obtained by a second order accurate leap frog solution of the envelope equation using 80 steps per lattice period. To check accuracy several runs with 160 steps per period were made; at $\alpha = 4$ the computed values of a/a_0 changed by $\sim 5 \times 10^{-6}$ and λ by 1.0×10^{-4}. Note that a maximum growth rate of only 11% per period appears in the first stop band ($\phi = 180°$).

5.4 Cold Fluid Model For Aberrations

The envelope equation derived in Section 5.1 essentially assumes that transverse forces are linear in the coordinate r and longitudinal forces are independent of r. The conservation of transverse emittance is a consequence of these approximations. It is clear, however, that non-linear components of force are present, especially in the fringe fields of the solenoids and in locations where strong accelerating fields are applied. Even the transverse oscillations of a mismatched beam envelope in a uniform field are subject to some non-linearity from space change fields and non-paraxial effects. The magnitude of these aberrations can be estimated from a cold fluid model of the beam dynamics which is presented in this subsection.

We consider an axisymmetric, time-independent system; the cold beam variables and fields depend only on coordinates r and z, and total current I is a constant. Each ion's canonical angular momentum $\underline{P}_\theta$ is conserved and is assumed to vanish:

$$0 = \underline{P}_\theta = r\left(Mv_\theta + qe\,A_\theta\right) \quad , \tag{78}$$

where A_θ (r, z) is the θ component of vector potential and satisfies

$$\frac{\partial}{\partial r}\frac{1}{r}\frac{\partial}{\partial r} r\,A_\theta + \frac{\partial^2 A_\theta}{\partial z^2} = 0 \tag{79}$$

inside the transport channel. The beam is a negligible source for A_θ, and the longitudinal component A_z may be neglected for the non-relativistic heavy ion application. The radial component A_r is eliminated as a gauge condition.

Particle energy (kinetic + potential) is also conserved and assumed to vanish:

$$0 = W = \frac{M}{2}\left(v_r^2 + v_\theta^2 + v_z^2\right) + qe\phi \quad , \tag{80}$$

where the scaler potential ϕ is related to beam charge density ρ in the channel by

$$\frac{1}{r}\frac{\partial}{\partial r} r\frac{\partial \phi}{\partial r} + \frac{\partial^2 \phi}{\partial z^2} = -\frac{\rho}{\varepsilon_0} \quad . \tag{81}$$

The conservation of W follows from the independence from time, as does the conservation of total current I. The continuity equation for current density $\vec{J} = \rho\vec{v}$ can therefore be written:

$$0 = \vec{\nabla}\cdot\vec{J} = \frac{1}{r}\frac{\partial}{\partial r} r\,\rho\,v_r + \frac{\partial}{\partial z}\rho\,v_z \quad . \tag{82}$$

So far we have five equations for the six functions v_r, v_θ, v_z, ρ, A_θ, ϕ. The necessary sixth independent equation could be either the r or z component of the force:

$$\vec{v}\cdot\vec{\nabla}\vec{v} = \frac{qe}{M}\left(\vec{E} + \vec{v}\times\vec{B}\right) \tag{83}$$

with

$$\vec{E} = -\vec{\nabla}\phi \quad , \tag{84}$$

$$\vec{B} = \vec{\nabla} \times A_\theta \hat{e}_\theta \quad . \tag{85}$$

However, an equivalent, and simpler sixth equation is:

$$\frac{\partial v_z}{\partial r} = \frac{\partial v_r}{\partial z} \quad , \tag{86}$$

which results from the conservation of fluid vorticity

$$0 = \vec{\nabla} \times \left(\vec{v} + \frac{qe}{M} \vec{A} \right) \quad , \tag{87}$$

which is also assumed to vanish at the beam source. This property is a consequence of the assumptions that the beam is a cold fluid with laminar flow.

It is convenient to absorb the constant factor qe / M into the definitions:

$$\frac{qe}{M} A_\theta \equiv A(r, z) \quad , \tag{88a}$$

$$\frac{qe}{M} \phi \equiv \Phi(r, z) \quad , \tag{88b}$$

$$\frac{qe}{M} \frac{\rho}{\varepsilon_0} \equiv R(r, z) \quad , \tag{88c}$$

$$v_r \equiv u(r, z) \quad , \tag{88d}$$

$$v_z \equiv v(r, z) \quad . \tag{88e}$$

Then we have after eliminating $v_\theta = -A$:

$$\frac{\partial}{\partial r} \frac{1}{r} \frac{\partial}{\partial r} r A + \frac{\partial^2 A}{\partial z^2} = 0 \quad , \tag{89}$$

$$\left(u^2 + A^2 + v^2 \right) + 2\Phi = 0 \quad , \tag{90}$$

$$\frac{1}{r} \frac{\partial}{\partial r} r \frac{\partial \Phi}{\partial r} + \frac{\partial^2 \Phi}{\partial z^2} = -R \quad , \tag{91}$$

$$\frac{1}{r}\frac{\partial}{\partial r}\, r\, Ru + \frac{\partial}{\partial z}\, Rv = 0 \quad , \qquad (92)$$

$$\frac{\partial v}{\partial r} - \frac{\partial u}{\partial z} = 0 \quad . \qquad (93)$$

In order to distinguish aberrations from the primary (linear theory) quantities, we expanded (A, Φ, R, u, v) in powers of r:

$$A = A_1\, r + A_3\, r^3 + \ldots\ldots \quad , \qquad (94a)$$

$$\Phi = \Phi_0 + \Phi_2\, r^2 + \ldots\ldots \quad , \qquad (94b)$$

$$R = R_0 + R_2\, r^2 + \ldots\ldots \quad , \qquad (94c)$$

$$u = u_1\, r + u_3\, r^3 + \ldots\ldots \quad , \qquad (94d)$$

$$v = v_o + v_2\, r^2 + \ldots\ldots \quad . \qquad (94e)$$

The coefficients A_1, A_3, Φ_0, etc, are functions only of z, and the associated powers of r are readily identified by an examination of eqns (89) - (93). Plugging the expansions 94(a - f) into these equations and equating coefficients of each power of r, we first obtain a low order set of five coupled equations relating the seven functions $(A_1, \Phi_0, \Phi_2, R_0, u_1, v_0, v_2)$:

$$v_o^2 + 2\Phi_0 = 0 \quad , \qquad (95)$$

$$\left(u_1^2 + A_1^2 + 2v_0\, v_2\right) + 2\Phi_2 = 0 \quad , \qquad (96)$$

$$4\,\Phi_2 + \Phi_0'' = -R_0 \quad , \qquad (97)$$

$$2R_0\, u_1 + \left(R_0\, v_0\right)' = 0 \quad , \qquad (98)$$

$$2v_2 - u_1' = 0 \quad . \qquad (99)$$

Two of the low-order functions can be specified arbitrarily; it is convenient to let these be $A_1(z)$ and $v_0(z)$. Note that the solenoidal on-axis field $\left(B_{z_0}\right)$ is related to A_1 by:

$$A_1(z) = \frac{qe}{2M} B_{z_0}(z) \quad , \qquad (100)$$

i.e., A_1 is the on-axis value of the Larmor frequency.

Equations (95) - (99) are essentially solved by determining the beam envelope radius a (z). To see this we define a (z) by the relation:

$$\frac{v_0\, a'}{a} \equiv u_1 \qquad (101)$$

This looks reasonable and defines a (z) to within a multiplicative constant. Equation (98) can then be integrated, yielding

$$R_0\, v_0\, a^2 = \text{constant} = \frac{qe}{M\varepsilon_0}\,\frac{I}{\pi} \qquad (102)$$

This value of the integration constant fixes a (z) to be close to the actual beam edge (but they are not exactly equal-- due to higher order contributions to J_z from R_2, v_2, R_4, v_4, . . .). From equation (99) we find that the second order longitudinal velocity coefficient:

$$v_2 = \frac{u_1'}{2} = \left(\frac{v_0\, a'}{2a}\right)' \qquad (103)$$

vanishes for constant a. This proves (in second order) the assertion that v_z is independent of r in Brillouin flow. Note that v_2 is an aberration coefficient that is obtainable directly from the envelope solution a(z) and is always present when the envelope oscillates. Fortunately, it disappears when oscillations are stopped by the application of matching elements in the beam line.

Eliminating v_2 and Φ_2 from equation (96), we have

$$\left(\frac{v_0\, a'}{a}\right)^2 + A_1^2 + 2v_0\left(\frac{v_0\, a'}{2a}\right)' + 2\left[-\frac{R_0}{4} - \frac{\Phi_0''}{4}\right] = 0 \qquad (104)$$

Substituting from equations (95), (100) and (102) gives:

$$\left(\frac{qe\, B_{z_0}}{2M}\right)^2 + v_0\left(\frac{v_0'\, a'}{a} + \frac{v_0\, a''}{a}\right) - \frac{1}{2}\,\frac{qe\, I}{M\varepsilon_0\pi}\,\frac{1}{v_0\, a^2} + \frac{v_0^{2''}}{4} = 0. \qquad (105)$$

Multiplication by a / v_0^2 and arranging terms yields an envelope equation:

$$a'' + \frac{v_0'}{v_0}\, a' = -\left(\frac{qeB_{z_0}}{2Mv_0}\right)^2 a + \left(\frac{2qe\, I}{4\pi\,\varepsilon_0\, Mv_0^3}\right)\frac{1}{a} - \frac{v_0^{2''}}{4v_0^2}\, a \qquad (106)$$

This is identical with equation (30) of Section 5.1 when emittance and canonical angular momentum are set equal to zero.

A set of five equations for the five next higher order expansion coefficients $(A_3, \Phi_4, R_2, u_3, v_4)$ is obtained in similar fashion to the lower order quantities:

$$8A_3 + A_1'' = 0 \quad , \tag{107}$$

$$2u_1 u_3 + 2A_1 A_3 + 2v_0 v_4 + v_2^2 + 2\Phi_4 = 0 \quad , \tag{108}$$

$$16\Phi_4 + \Phi_2'' = -R_2 \quad , \tag{109}$$

$$4\left(R_2 u_1 + R_0 u_3\right) + \left(R_2 v_0 + R_0 v_2\right)' = 0 \quad , \tag{110}$$

$$4v_4 - u_3' = 0 \quad . \tag{111}$$

These aberration coefficients are "excited" by various lower order disturbances such as acceleration and changes in B_{z_0}. As an example of the application of equations (107) - (111) we return to the periodic solenoidal field treated in 5.3, but assuming v_0 and Q are constant. We have

$$A_1 = \frac{qe}{2M} B_{z_0}(z) = \frac{k_{c_0} v_0}{2}(1 + \varepsilon \cos Kz) \quad , \tag{112}$$

$$a \equiv a_0\left(1 + \frac{\varepsilon \cos Kz}{\alpha - 1}\right) \quad , \tag{113}$$

where

$$\alpha = 2K^2 / k_{c_0}^2 \quad .$$

Working to lowest order in ε, it follows that

$$\frac{v_r}{v_0} \equiv \frac{u_1 r}{v_0} + \frac{u_3 r^3}{v_0} + \ldots.$$

$$\equiv -(Ka_0)\left(\frac{\varepsilon \sin Kz}{\alpha - 1}\right)\left[\left(\frac{r}{a_0}\right) + \frac{(Ka_0)^2}{4}\left(\frac{r}{a_0}\right)^3\right] \quad , \tag{114}$$

$$\frac{J_z}{\left(I/\pi a^2\right)} = \left(\frac{\pi M \varepsilon_0}{qeI}\right)\left(R_0 + R_2 r^2 + \ldots.\right)\left(v_0 + v_2 r^2 + ..\right)a^2$$

$$\approx 1 - (Ka_0)^2\left(\frac{\varepsilon \cos Kz}{\alpha - 1}\right)\left(\frac{r}{a_0}\right)^2 \quad , \tag{115}$$

$$\frac{qe\phi}{-Mv_0^2/2} = 1 - \frac{2}{v_0^2}\left(\Phi_2 r^2 + \Phi_4 r^4 + ..\right)$$

$$\approx 1 + \frac{\left(k_{c_0} a_0\right)^2}{4}\left[\left(1 - \frac{2\varepsilon \cos Kz}{\alpha - 1}\right)\left(\frac{r}{a_0}\right)^2 - \frac{(Ka_0)^2}{4}\left(\frac{\varepsilon \cos Kz}{\alpha - 1}\right)\left(\frac{r}{a_0}\right)^4\right] \quad . \qquad (116)$$

These are the matched (periodic) aberrations that necessarily accompany the matched oscillations of the beam; they do not grow. Note that the non-linear parts are small by factors of $(Ka_0)^2$ as well as ε. However, all coefficients blow up as $\alpha \to 1$, as might be expected from the discussion in Section 5.3. Assuming typical values $\varepsilon = 0.2, Ka_0 = 0.5, k_{c_0} a_0 = 0.25$, corresponding to $\alpha = 8.0$, the nonlinear portions of expressions for v_r, J_z, ϕ are relatively of magnitude

$$\left(\frac{v_r}{v_0}\right)_{NL} \sim 9 \times 10^{-4} \quad ,$$

$$\left(\frac{J_z}{I/\pi a^2}\right)_{NL} \sim 7 \times 10^{-3} \quad ,$$

$$\left(\frac{qe\phi}{-Mv_0^2/2}\right)_{NL} \sim 3 \times 10^{-5} \quad .$$

6. Concluding Remarks

Based on this preliminary study, the solenoidal transport option for the IRE seems worthy of further serious consideration. Analysis of the elementary, axisymmetric dynamics indicates that high ion currents might be transported with relatively minor envelope oscillations. A conceptual design of the high voltage injector is required before selecting a final set of beam parameters, but the engineering maturity of the superconducing solenoids and the acceleration subsystems should allow realistic cost estimates to be prepared when this is done. The critical judgement will ultimately be the relative risks of meeting the emittance and brightness goals with the single high current beam channel, compared with confining beams from multiple channels. Further physics study would help make this a more informed decision.

Acknowledgement

We authors benefited from the advice of Clyde Taylor and Ronald Scanlan on the superconducting magnet technology, and William Herrmannsfeldt on injector optics design. Enrique Henestroza made computations which helped elucidate the peculiarities of the matched envelope near $\phi = 360°$. Andris Faltens and Roger Bangerter provided much valuable and stimulating advice on the utility of solenoids and associated issues.

References

1. W. Barletta, A. Faltens, E. Henestroza, and E. Lee, "High Current Induction Linacs", Accelerator Driven Transmutation Technology Conference, Las Vegas, NV, July 25-29, 1994.
2. Elise Conceptual Design Report, Lawrence Berkeley National Laboratory PUB-5393, pgs 1-5 and 1-6, February, 1994.
3. C.M. Celata, A. Faltens, D.L. Judd, L. Smith, and M.G. Tiefenback, "Transverse Combining of Nonrelativistic Beams in a Multiple Beam Induction Linac", 1987 Particle Accelerator Conference, Washington, D.C., March 16-18, 1987, pg. 1167-1169.
4. J. Hovingh, V. Brady, A. Faltens, D. Keefe, and E. Lee, "Heavy-Ion Linear Induction Accelerators as Drivers for Inertial Fusion Power Plants", Fusion Technology Vol. 13, pg 255-278, February 1988.
5. Technology Options Study for the Second Axis of DARHT, report by LBNL in preparation, 1997.
6. J.D. Lawson, The Physics of Charged Particle Beams, Clarendon Presss, Oxford, 1978.
7. R.C. Davidson, Physics of Nonneutral Plasmas, Addison Wesley 1990.
8. M. Reiser, Theory and Design of Charged Particle Beams, John Wiley & Sons, 1994.

Ernest Orlando Lawrence Berkeley National Laboratory
One Cyclotron Road | Berkeley, California 94720

Prepared for the U.S. Department of Energy under Contract No. DE-AC03-76SF00098